An interlaboratory comparison on the characterization of a sub-micrometer polydisperse particle dispersion

Benkstein, K.D.; Balakrishnan, G.; Bhirde, A.; Chalus, P.; Das, T.K.; Do, N.; ... ; Yang, D.

Journal of Pharmaceutical Sciences 000 (2021) 1–11

Contents lists available at ScienceDirect

Journal of Pharmaceutical Sciences

journal homepage: www.jpharmsci.org

Pharmaceutical Biotechnology

An Interlaboratory Comparison on the Characterization of a Sub-micrometer Polydisperse Particle Dispersion

Kurt D. Benkstein[a,*], Gurusamy Balakrishnan[b], Ashwinkumar Bhirde[c], Pascal Chalus[d], Tapan K. Das[e], Ngoc Do[f], David L. Duewer[g], Nazar Filonov[h,i], Fook Chiong Cheong[j], Patrick Garidel[k], Nicole S. Gill[l], Adam D. Grabarek[m,n], David G. Grier[o], Judith Hadley[p], Andrew D. Hollingsworth[o], Wesley W. Howard[q], Maciej Jarzębski[r], Wim Jiskoot[s], Sambit R. Kar[e,1], Vikram Kestens[t], Harshit Khasa[q], Yoen Joo Kim[q], Atanas Koulov[d], Anja Matter[d], Laura A. Philips[j], Christine Probst[u,1], Yannic Ramaye[t], Theodore W. Randolph[v], Dean C. Ripple[a], Stefan Romeijn[s], Miguel Saggu[w], Franziska Schleinzer[k], Jared R. Snell[v,1], Jan "Kuba" Tatarkiewicz[x], Heather Anne Wright[l,1], Dennis T. Yang[y]

[a] *Biomolecular Measurement Division, National Institute of Standards and Technology, Gaithersburg, MD 20899, USA*
[b] *Analytical Development and Attribute Science, Bristol Myers Squibb, New Brunswick, NJ 08901, USA*
[c] *Office of Biotechnology Products, Office of Pharmaceutical Quality, Center for Drug Evaluation and Research, U.S. Food and Drug Administration, 10903 New Hampshire Avenue, Silver Spring, MD 20993, USA*
[d] *Lonza AG, Drug Product Services, Hochbergerstrasse 60G, CH-4057 Basel, Switzerland*
[e] *Biologics Development, Bristol Myers Squibb, New Brunswick, NJ 08903, USA*
[f] *Spectradyne LLC, 23875 Madison St Suite A, Torrance CA 90505, USA*
[g] *Chemical Sciences Division, National Institute of Standards and Technology, Gaithersburg, MD 20899, USA*
[h] *AlphaNanoTech, Morrisville, NC 27709, USA*
[i] *Particle Metrix, Inc., Mebane, NC 27302, USA*
[j] *Spheryx, Inc., New York, NY 10016, USA*
[k] *Boehringer Ingelheim Pharma GmbH & Co. KG, Innovation Unit, PDB, D-88397 Biberach an der Riss, Germany*
[l] *Yokogawa Fluid Imaging Technologies, Inc. Scarborough, ME 04074, USA*
[m] *Coriolis Pharma, Fraunhoferstrasse 18 b, 82152 Martinsried, Germany*
[n] *Division of BioTherapeutics, Leiden Academic Centre for Drug Research, Leiden University, The Netherlands*
[o] *Department of Physics and Center for Soft Matter Research, New York University, New York, NY 10003, USA*
[p] *Malvern Pananalytical, 117 Flanders Road Westborough, MA 01581, USA*
[q] *Analytical Sciences, BioPharmaceuticals Development, R&D, AstraZeneca, Gaithersburg, USA*
[r] *Department of Physics and Biophysics, Faculty of Food Science and Nutrition, Poznan University of Life Sciences, Poznan, Poland*
[s] *Division of BioTherapeutics, Leiden Academic Centre for Drug Research, Leiden University, Leiden, the Netherlands*
[t] *European Commission, Joint Research Centre (JRC), Geel, Belgium*
[u] *Luminex Corporation, Seattle, WA 98119, USA*
[v] *Department of Chemical and Biological Engineering, University of Colorado, Boulder, CO 80309*
[w] *Pharmaceutical Development, Genentech, Inc., 1 DNA Way, South San Francisco, CA 94080, USA*
[x] *HORIBA Scientific, Irvine, CA 92618, USA*
[y] *Biopharmaceutical Research and Development, Lilly Research Laboratories, Eli Lilly and Company, Indianapolis, IN 46285, USA*

Abbreviations: AFM, atomic force microscopy; CDD, concentration distribution density; CV, coefficient of variation; DLS, dynamic light scattering; EM, electron microscopy; ESZ, electrical sensing zone; ETFE, ethylene tetrafluoroethylene; HPC, holographic particle characterization; ILC, interlaboratory comparison; mCV, mean coefficient of variation; OTH, group of other instrument types with smaller numbers of datasets; PdP, polydisperse particles; PETG, polyethylene terephthalate glycol; PMMA, poly(methyl methacrylate); PNC, particle number concentration; PS, polystyrene; PTA, particle tracking analysis; RMM, resonant mass measurement; SAXS, small angle X-ray scattering; TEM, transmission electron microscopy.

Disclaimer: This manuscript reflects the views of the authors and should not be construed to represent FDA's views or policies.

* Corresponding author at: Biomolecular Measurement Division, National Institute of Standards and Technology, 100 Bureau Dr, MS 8362, Gaithersburg, MD 20899, United States.
E-mail address: kurt.benkstein@nist.gov (K.D. Benkstein).

[1] No longer at this institution.

https://doi.org/10.1016/j.xphs.2021.11.006
0022-3549/

ARTICLE INFO

Article history:
Received 13 August 2021
Revised 10 November 2021
Accepted 10 November 2021
Available online xxx

ABSTRACT

The measurement of polydisperse protein aggregates and particles in biotherapeutics remains a challenge, especially for particles with diameters of ≈ 1 μm and below (sub-micrometer). This paper describes an interlaboratory comparison with the goal of assessing the measurement variability for the characterization of a sub-micrometer polydisperse particle dispersion composed of five sub-populations of poly(methyl methacrylate) (PMMA) and silica beads. The study included 20 participating laboratories from industry, academia, and government, and a variety of state-of-the-art particle-counting instruments. The received datasets were organized by instrument class to enable comparison of intralaboratory and interlaboratory performance. The main findings included high variability between datasets from different laboratories, with coefficients of variation from 13 % to 189 %. Intralaboratory variability was, on average, 37 % of the interlaboratory variability for an instrument class and particle sub-population. Drop-offs at either end of the size range and poor agreement on maximum counts of particle sub-populations were noted. The mean distributions from an instrument class, however, showed the size-coverage range for that class. The study shows that a polydisperse sample can be used to assess performance capabilities of an instrument set-up (including hardware, software, and user settings) and provides guidance for the development of polydisperse reference materials.

Introduction

The development and clinical application of protein-based biotherapeutics continues to expand. Because these biotherapeutics are based on large, flexible, and dynamic molecules, they are subject to aggregation that can be exacerbated by various physical and chemical stressors.[1-5] Aggregation can ultimately lead to the formation of particulates that can affect the efficacy, stability, and safety of the drug product.[1,3-6] The particulates can be classified in a number of ways, with size (e.g., length, equivalent spherical diameter, Feret diameter, volume) being one of the more common parameters. Size (diameter) ranges are commonly divided into visible (> 100 μm), subvisible (0.1 μm to 100 μm), and oligomers (< 0.1 μm).[1,2] The particle size ranges can also be classified in different ways based on the measurement technique used, for example light obscuration and optical flow imaging techniques are capable of measuring subvisible particles in the range of (1 to 100) μm. The range from 0.1 μm to 1 μm can be further classified as a sub-micrometer size regime; this range is of particular interest in the biopharmaceutical field for understanding the aggregation of the therapeutic proteins and potential implications on immunogenicity.[2,7-10] Identifying non-proteinaceous particles in the sub-micrometer size regime (e.g., silicone oil droplets, steel or other intrinsic materials related to therapeutic processing and extrinsic materials) is also of interest,[7,11] while other types of samples have similar challenges and interests (e.g., hydrocolloids and food structures, drug and vaccine delivery systems, or extracellular vesicles).[12-15]

Particles with sizes (equivalent diameters) below ≈ 1 μm are particularly challenging to count and size, given the cutoff for typical optical flow imaging and light obscuration analysis tools.[16] Many commonly used approaches for characterizing particles in biotherapeutics have limited utility in this range (e.g., light obscuration is used for larger particles, size exclusion chromatography is typically used for protein monomers, dimers, and oligomers, and other small particles such as viruses and virus-like particles, and nanomaterials). Analysis is further complicated by the polydisperse nature and possible chemical heterogeneity of the particles.[2,8,16,17]

Given these challenges in characterizing sub-micrometer particulates in biotherapeutics, relatively new technologies have been developed (e.g., particle tracking analysis, resonant mass measurement, holographic particle characterization) and several other techniques have been adapted (e.g., electrical sensing zone, flow imaging, flow cytometry).[18-20] The performance of particle counting and sizing instruments is often evaluated by using particle populations that are well characterized and stable. Polystyrene latex and silica beads are common choices, because generation of stable protein particle materials is difficult.[21] Comparisons of orthogonal instruments and interlaboratory comparisons (ILCs) have been undertaken using single populations of beads to evaluate the performance of instruments used to size and count sub-micrometer particles.[10,22-27] Because these particles tend to be monodisperse, using a single particle population does not necessarily characterize the full range of an instrument response. Several of these ILC studies have included extensions to bimodal populations,[22,23] or to polydisperse samples.[10] Furthermore, the idea of using a synthetic polydisperse (multimodal or picket fence) sample for characterizing instrument responses over larger size ranges has been discussed in the literature and in technical specifications intended for standardization documents.[15,28-32] For example, Gross et al. reported on a study using particle tracking analysis that characterized beads of 50 nm, 400 nm, and 600 nm.[30]

In this ILC, a sample of mixed particle populations was employed to assess the counting and sizing responses of several instrument types. The participating groups (Supplemental Table S1) in the study included seven instrument developers and seven industry, four academic, and three government laboratories. The sample was an aqueous distribution of beads from five different populations with nominal diameters ranging from (0.1 to 1) μm to cover the typical "sub-micrometer" size regime. The lower limit of 0.1 μm was chosen to be within the lower limits for many of the instrument types being used. The upper limit of 1 μm was chosen as it represents the size where well-established approaches such as light obscuration could be used. The goal was to capture the intralaboratory and interlaboratory variability in evaluating the particle number concentration (PNC) and size distributions of the polydisperse particle (PdP) dispersion. The strength of this study is built upon the combination of a polydisperse test sample, a varied selection of instrument types and approaches, and a large and varied participant group.

This paper reports trends in intralaboratory and interlaboratory variability for the different instrument types and provides a snapshot of comparability at the time of the measurements. To facilitate that approach, the datasets were grouped into four categories based upon the instrument types: (nano)particle tracking analysis (PTA), resonant mass measurement (RMM), electrical sensing zone (ESZ), and a collection of other instrument types (OTH) that had relatively few datasets. The OTH group included several methods that are typically used for micrometer-scale particles, but which are now capable of counting and characterizing particles of several hundred nanometers.

Experimental Section

Sample: The PdP dispersion was prepared at NIST by mixing five sphere populations that had different nominal sizes (0.1 μm ≤ d_{nom}

Table 1
Nominal particle diameters with coefficient of variation (CV) (from manufacturer datasheets; ± 1 standard deviation; diameter and size statistics from DLS (PMMA) or TEM analysis (silica)).

Particle material	Particle diameter (μm)	CV	Fractional population, targeted (by PNC)
PMMA	0.113 ± 0.016	15 %	0.66
silica	0.195 ± 0.012	5.9 %	0.22
PMMA	0.318 ± 0.048	15 %	0.08
PMMA	0.495 ± 0.126	25 %	0.03
PMMA	1.089 ± 0.230	21 %	0.01

≤ 1 μm; see Table 1) in purified water (resistivity of 18.2 MΩ·cm at 25 °C, 0.2 μm filter pore size) containing 0.02 % by mass of sodium azide as a bacteriostatic agent. The targeted combined PNC for all particles was ≈ 10^9 mL^{-1} based upon the manufacturer's estimated concentration (1 % solid content by mass for four populations of poly (methyl methacrylate) (PMMA) particles from Phosphorex[33] or 10.6 mg/mL for one population of silica particles from nanoComposix[33]). These numbers were used to estimate the final PNC for the sample and the approximate PNC ratios for each particle population (See Supplemental Table S2 for a summary of volumes used to prepare the sample). However, for the purpose of this ILC, ground truth values of the sizes and distribution counts were not established for the sample. Both PMMA and silica are sufficiently hydrophilic such that no surfactant is needed. In preliminary screenings, we found that samples without surfactant had better stability than those samples with surfactant over 5 months, with respect to PNC as measured by PTA. The source of the instability in PNC with the surfactant-based sample was not determined. The PNC for the surfactant-free dispersion was tracked over 12 months and yielded stable values (see Supplemental Figure S1). The number concentration of each sphere population was targeted to a power law distribution such that as the diameter (d_{nom}) of the sphere increased, its nominal PNC would decrease as approximately $1/d_{nom}^2$ (Table 1).[8] The stock dispersion was divided into 50 samples, each with 20 mL of the dispersion in 30 mL PETG (polyethylene terephthalate glycol) media bottles, and stored at 4 °C. The samples were distributed as pairs to the participating laboratories (see Supplementary Materials for a discussion of the Youden method of determining variability using sample pairs). A blank sample (purified water with 0.02 % sodium azide) was also included in the shipment. Shipping containers included a freeze indicator: in one case, samples arrived with the freeze indicator activated, and a replacement sample was shipped.

General handling instructions were included with the sample. These instructions included recommendations on storage, resuspension, sampling, and dilution. Samples were to be stored between (2 and 8) °C in the dark, and allowed to come to room temperature before sampling. To resuspend the samples, the bottles were to be agitated (with inversion) for 20 s followed by sonication for 20 s. Prior to sampling from bottles, the bottles were to be gently tipped from side to side 20 times while rotating. For sampling by pipet, it was recommended that the tip be located in the middle of suspension. Samples could be diluted immediately prior to analysis, and it was noted that a series of dilutions may be necessary to find an appropriate concentration range for a specific instrument or analysis approach.

Measurements: Beyond the sample handling instructions above, the choice of methods and the exact pattern of replicates, measured volumes, measuring protocols, etc. was left to each participating laboratory.[21] For each set of measurements, the participants could limit the range of diameters for which data were reported, based on the assessment of the working range and measurement reliability of the instrument used, the reproducibility of the data, or the statistical significance of the obtained particle counts. Participants were asked to measure and report the data within one month of receipt of the sample. When this deadline was not feasible, laboratories were asked to make an initial measurement upon receipt of the sample to compare with later measurements for documenting changes to the sample. Participants were provided a data template that requested particle number concentrations for bins 10 nm wide ranging between 0.05 μm and 2 μm (or as appropriate for the measurement method). In addition to the PNC as a function of particle size, the data template also provided space for entries on the basis of calibration (laboratories typically employed monodisperse polystyrene size standards to verify performance), the dilution factor, the number of replicate measurements, the nominal measured volume, and the average total particles counted per run, as well as any other settings relevant to the method used.

Specific summaries by instrument group are given in the following paragraphs. The dataset reflects measurements that were made between late fall of 2018 and early spring of 2019. Data reports were received from December 2018 through April 2019.

The PTA group had 18 paired datasets and included instruments from three different manufacturers (HORIBA Scientific, Malvern Panalytical, and Particle Metrix).[33] The different models included ViewSizer 3000 (HORIBA), LM10, LM14, LM20, NS300, and NS500 (Malvern Panalytical), and the ZetaView and ZetaView Duo (Particle Metrix).[33] Amongst all of the instruments, nine different versions of acquisition/analysis software were used. Participants were asked to provide information on settings specific to PTA such as camera gain, shutter speed, and imaging efficiency.

The RMM group had seven paired datasets and was composed of instruments from a single manufacturer and model: Archimedes from Malvern Panalytical.[33] Variables between laboratories included the sensor used, the software version, and the total number of particles analyzed. All laboratories used the density of PMMA for the size analysis, and where specified, a 1 μm polystyrene bead for calibration. The position of the silica beads is expected to shift for the RMM measurements by the ratio of the buoyant densities of silica and PMMA, to the 1/3 power:

$$d_{expected} = d_{silica}\left(\frac{(\rho_{silica} - \rho_{water})}{(\rho_{PMMA} - \rho_{water})}\right)^{1/3} \quad (1)$$

For a silica bead with a diameter d_{silica} = 0.195 μm and density ρ_{silica} = 2.0 g/mL, given a PMMA density of ρ_{PMMA} = 1.19 g/mL and water density (ca. room temperature) ρ_{water} = 1.0 g/mL the expected RMM diameter $d_{expected}$ is ≈ 0.35 μm.

The ESZ group had four paired datasets and was composed of instruments from two manufacturers: the nCS1 from Spectradyne and the Multisizer 4 from Beckman Coulter.[33] Variables between laboratories included the orifice size, which directly impacted the size limits for detecting particles, analysis software, and diluent. In some instances data were acquired using multiple orifice sizes to expand the size coverage range.

The OTH group had seven paired datasets from a diverse set of instruments, which included three xSight from Spheryx (holographic particle characterization, HPC), one FlowCam Nano from Yokogawa Fluid Imaging Technologies (flow-imaging microscopy), and one SALD7500-nano from Shimadzu (quantitative laser diffraction).[33] The results from two flow cytometer instruments from Amnis® (CellStream® and FlowSight®)[33] were also included in this group for analysis using the "large bins" (see *Data analysis* below).

The overall numbers are summarized in Supplemental Table S3.

Data analysis: Data received from the study participants were anonymized and if necessary adjusted for dilution. For comparisons between the laboratories and the techniques, the particle size distributions, when feasible, were adjusted to use a "rounded log" for the

Table 2
Large bin size ranges.

Bin	Particle size range	Bin width (nm)
Bin1	$d < 0.14\ \mu$m	90
Bin2	$(0.14 \le d < 0.23)\ \mu$m	90
Bin3	$(0.23 \le d < 0.44)\ \mu$m	210
Bin4	$(0.44 \le d < 0.86)\ \mu$m	420
Bin5	$0.86\ \mu\text{m} \le d$	1200

bin widths: 10 nm bins starting at d = 0.050 μm (left edge) to 0.44 μm, 30 nm bins from 0.44 μm to 0.86 μm, and 100 nm bins from 0.86 μm and larger. For datasets that had bin edges that were offset or did not otherwise match the common spacing, an interpolation was performed on the cumulative particle size distributions to align with the common bin edges for clarity in presentation and to facilitate comparisons. The particle number concentrations were then divided by the bin width to provide concentration distribution density (CDD) with units of ($mL^{-1}nm^{-1}$). Using the variable bin widths across the entire size range preserves diameter sensitivity at small sizes while reducing statistical noise at large sizes. Converting to CDD gives a number concentration measure that is normalized to the bin width. Mean distributions were generated using only datasets that provided a number for a particular size bin. Standard errors of the mean were calculated by dividing the standard deviation of the mean by the square root of the number of laboratories contributing datasets for a particular bin because of the high correlation between datasets from the same laboratory. The particle size distributions were also organized into "large bins" (Table 2), based upon the nominal particle sub-population diameters. These large bins facilitated the analysis of intralaboratory and interlaboratory variability by reducing the complexity. The large bins dataset also included two additional measurements in the OTH group from flow cytometers that did not have sufficient resolution for the "rounded log" distributions but could be collected into the larger bins, with offsets to the bin edges (see dataset in Supplemental Materials). Outliers observed in the Youden plots (see Supplemental Materials) were examined for statistical significance (i.e., whether more than 10 measured particles contributed to the counts in the large bins). One distribution pair in the PTA group (D31) had Bin5 counts that showed up as outliers and had measured less than 10 particles. The numbers from that dataset were not included in the analyses that used Bin5.

Results

Representative concentration distribution density (CDD) plots from the varied datasets are shown in Fig. 1 for the four technique groups (see Supplemental Figure S2 for the distributions shown with a linear y-scale). Across all the datasets, different particle size ranges were measured since the varied instrument types and data acquisition settings had different operational ranges with respect to particle sizes (Fig. 1 and Supplemental Figure S2 with Supplemental Figure S3 showing the complementary cumulative PNCs for the datasets plotted in Fig. 1). From the plots of the concentration distribution densities within instrument groups, differences between datasets on the measurements and particle sizes counted are apparent as well. Such differences are most apparent where the particle count in a bin drops out, that is, where the particle CDD goes to 0 $mL^{-1}nm^{-1}$, but differences are also evident in bins where all datasets within an instrument group show a non-zero CDD value. This can be observed in the PTA group in Fig. 1 where there are CDD differences of a factor of 100 or more across the datasets. Although there were multiple instrument types and software versions within the PTA group especially, there was an insufficient number of instruments to delve into the specifics of instrument model or software version. Because of the typical instrument limitations in the size regime probed in this study, not all datasets reported on the full range of particles sizes.

The mean particle size distributions for each instrument group were calculated, which included the distributions for the two identical samples. Within the OTH group, because of the diverse nature of the instruments used to collect the datasets, a global mean distribution was not calculated; however, the mean of the three paired datasets from instruments using HPC was calculated. The mean distributions are shown with their respective instrument groups in Fig. 1 and combined in Fig. 2. The individual datasets tended to have limited coverage and generally did not measure the CDD over the full (0.1 to 1.0) μm size range. However, the mean distributions of the combined overlapping datasets shown in Fig. 2 suggest that instrumental coverage is sufficiently broad to measure particles across the entirety of the sub-micrometer size regime of this sample.

Distinct peaks are evident in the mean distributions (Fig. 2), which generally correspond to the sizes of each of the added particle populations (arrows in the plots, Table 1). For the techniques that do not cover the full range of particle sizes (with the smaller particles generally being below the size limits for a particular instrumental configuration), lesser numbers of peaks are observed. The linear and logarithmic scales highlight the capabilities of the various techniques for smaller and/or larger sub-micrometer particles. The mean distributions display similar trends in each of the instrument groups, i.e., showing decreasing CDDs with increasing particle diameter. The PTA and ESZ techniques show high counts for particles with $d < 0.5\ \mu$m. The instruments in the RMM and OTH groups show counts for larger particles. For the smaller particles in the mixture, the RMM mean distribution shows falling CDD for particle diameters below d = 0.28 μm, and zero counts for particle diameters below d = 0.19 μm. The HPC mean distribution in the OTH group shows falling CDD counts for particle diameters below d = 0.4 μm and zero counts for particle diameters below 0.3 μm. The other two distributions in the OTH group show rapid drops in CDD counts: for diameters below d = 0.25 μm (quantitative laser diffraction) and d = 0.19 μm (flow imaging microscopy). The inset of Fig. 2 shows that the PTA and ESZ techniques provide counts for the larger particles as well, with distinct peaks for the (0.5 and 1) μm particles, although the PTA mean distribution shows the peaks shifted to smaller particle diameters (e.g., the peak position for the largest particles in the PTA mean distribution is located in the bins for 0.63 μm and 0.65 μm particles). For the PTA instruments, the Brownian motion of the larger particles is relatively slow, so an instrument optimized for tracking the more abundant smaller particles (e.g., by using faster frame rates or higher camera sensitivities) may underestimate the size of the larger particles in the distribution (e.g., challenges in locating and tracking the particle center of mass).[34] The ESZ, RMM, and HPC mean instrument distributions all show a peak for the 1 μm particles with d_{avg} = (1.07 to 1.13) μm (Fig. 2, inset), which corresponds well with the nominal particle size (from the manufacturer) of $d = (1.089 \pm 0.230)\ \mu$m.

To simplify the comparison of the datasets, the particle number concentrations and concentration distribution densities for each dataset were organized into large bins centered around the nominal peak particle diameters (Table 2). This reduced the number of bins from 66 to five. Fig. 3 shows the distribution of log(CDD) numbers for each large bin and instrument group plotted as box-and-whisker plots. The CDD range (y-axis) for each panel is kept constant, to facilitate better comparisons between the distribution widths. The OTH instrument group is included in Fig. 3 for completeness but includes results from many different approaches that may be optimized for varied particle size ranges. Indeed, the spread of the points tends to be large, although similar instruments tend to show clusters in the plot. The "large bin" particle number concentrations are summarized

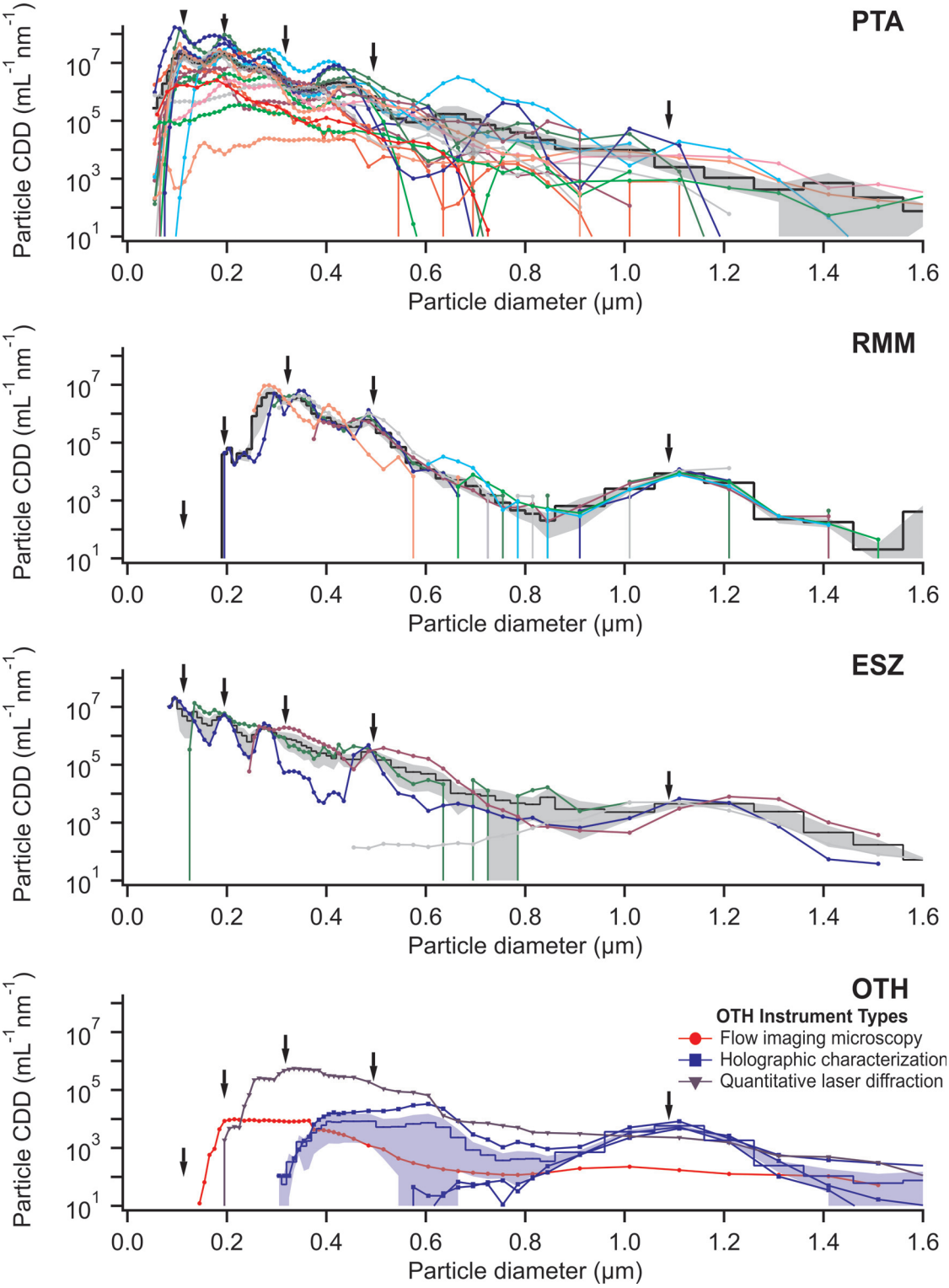

Figure 1. Concentration distribution density (CDD) plots for the PdP sample using a consistent logarithmic *y*-scale. For PTA, RMM, and ESZ, different datasets (one plot from each dataset pair, for clarity) are denoted by color within each figure, while for OTH, the different colors indicate different instrument types. The black step-distribution (PTA, RMM, ESZ) represents the mean of all the distributions within that technique group. The blue step-distribution (OTH) represents the mean of all HPC datasets. The datasets are plotted with points bin centered, while the mean distributions are plotted with steps based upon the bin left edge. The shading represents ± the standard deviation of the mean (i.e., standard error) for the step-distributions. The arrows indicate the nominal particle diameters (Table 1).

in Supplemental Figure S4 and Supplemental Table S4. These are presented as complementary cumulative particle number concentrations, i.e., the cumulative number of particles of a diameter greater than or equal to the bin size (left edge). Qualitatively, a downward trend in log(CDD) is expected in Fig. 3 as the sizes of the particles in the bins increase. For the PTA group, the data spread is indicated by the relatively large boxes (one order of magnitude and larger) and extended whiskers for each of the bin sizes. For Bin1, Bin2, and Bin3,

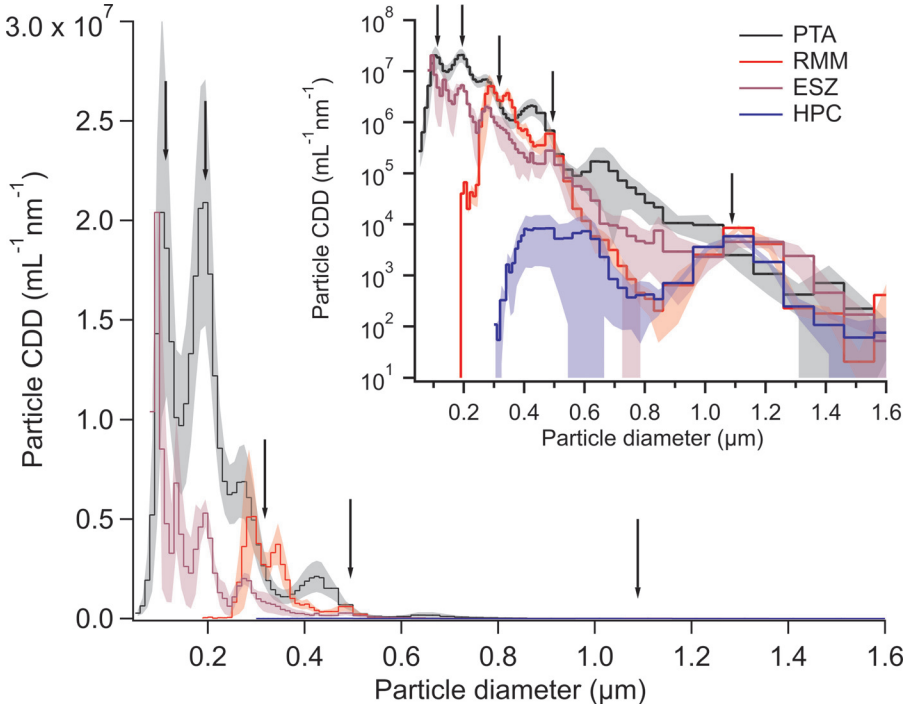

Figure 2. Mean concentration distribution density plots for the PdP sample from each of the technique groups. The HPC curve is the mean of the three paired datasets acquired using holographic particle characterization in the OTH group. The inset shows the same plot with a logarithmic *y*-axis to show the distribution of larger particles at lower particle concentration distribution densities. In cases where a distribution did not report PNC for a size bin, that distribution was not included in the calculations for the bin. The shading represents ± the standard error. The arrows indicate the nominal particle diameters.

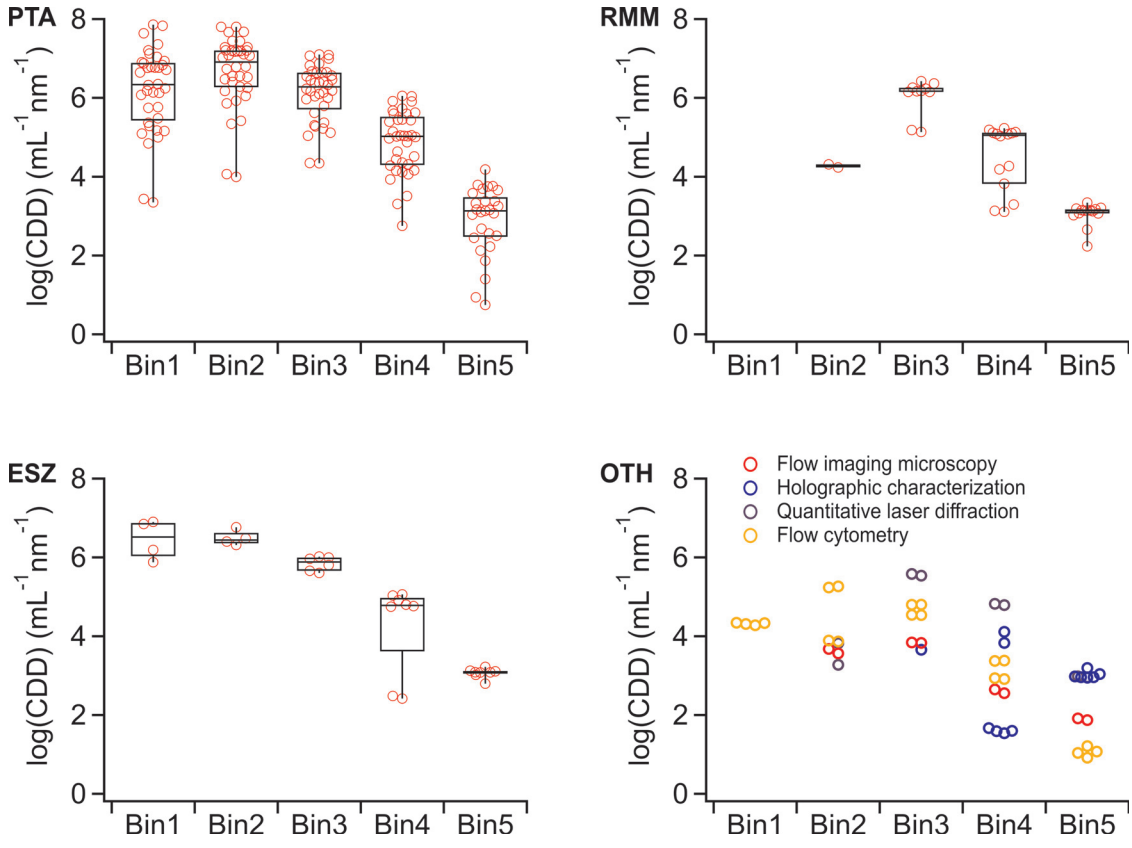

Figure 3. Box plots for the log of the particle concentration distribution density (CDD) for each technique group, broken down into particle size bins (See Table 2). The boxes represent the interquartile range (IQR), with the center line as the median particle CDD for that size bin and group. The whiskers extending above and below the boxes show the full spread of data points. For the OTH group, statistics were not calculated because of the diverse nature of the instruments; however the log(CDD)'s for each dataset are shown for reference, color-coded by instrument type.

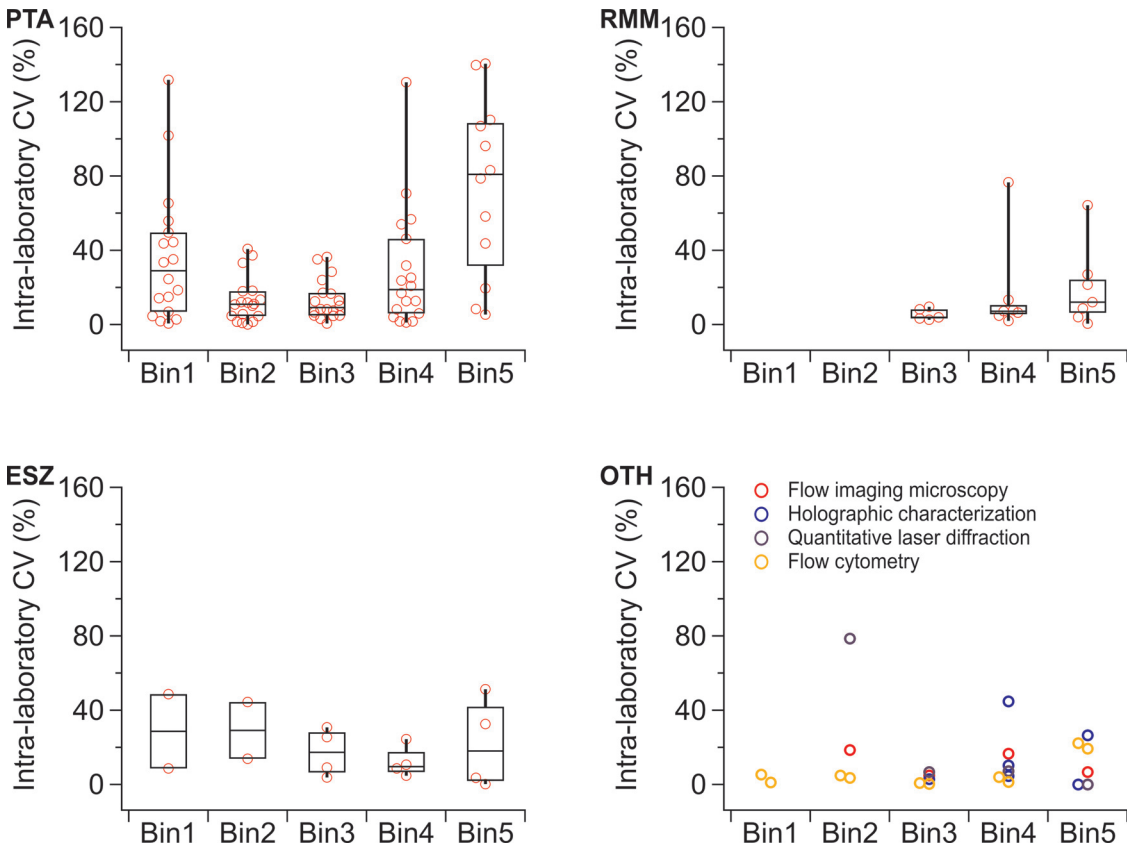

Figure 4. Box plots showing the range of intralaboratory CVs. The box plots show the median (center line), interquartile ranges (box tops and bottoms), and the extremes (whiskers). For the OTH group, box-plot summaries were not calculated because of the diverse nature of the instruments.

the lowest two values are all from the same laboratory; however for the larger particles in Bin4 and Bin5, the numbers from that laboratory are more in line with the other measurements.

The RMM and ESZ plots tend to show relatively smaller boxes, supporting the lower interlaboratory CVs for those groups (Table 4). The large spread observed for ESZ Bin4 is attributable to the measurements from a single laboratory that were much lower than the other laboratories (instrument with a particle size measurement range optimized for larger particles, i.e., Bin5). For the RMM group, the lowest two numbers are from the same laboratory, although the particular laboratory is different for data in each of Bin3, Bin4, and Bin5. A distinct downward trend in CDD per bin is observed for the PTA and ESZ groups from Bin2 through Bin5 (from Bin3 through Bin5 for the RMM group). The trends are confirmed by fitting a linear model to the mean log (CDD) values (Bins 3, 4, and 5 for the RMM group and all bins for the other groups). The center of the bins was used as the independent variable, and the fit was weighted with the standard deviations of the log(CDD). The PTA, RMM, and ESZ groups each showed a slope of -2.5 with standard deviations up to 0.8.

To quantify the intralaboratory and interlaboratory variability, the particle counts from the datasets organized into these large bins were compared. Because the OTH group featured many types of instruments, the statistical analysis focused on the three laboratories using holographic particle characterization (n = 3, HPC). The numbers from the other instruments in the OTH are still shown in the plots (Figs. 3, 4, S4, S5). The intralaboratory variabilities are shown in Table 3 for each instrument group. The distributions of CVs for each bin and instrument group is shown in the box plot (Fig. 4). The interlaboratory variability and the mean PNC by bin is summarized in Table 4. The box plots provide graphical summaries of the distribution of the CV and PNC data from each dataset pair. Box plots emphasize the quartile statistical distance of each number from the median, while the point positions show the distributions.

The intralaboratory CVs, summarized in Table 3, tend to be smaller than the interlaboratory CVs shown in Table 4, with 90 % of

Table 3
Intralaboratory variability: Coefficients of variation ($CV = \left(\frac{\sigma_{Lab}}{PNC_{mean,Lab}}\right)$, where σ_{Lab} is the standard deviation of the PNC between replicates 1 and 2 for laboratory *Lab*, and $PNC_{mean,Lab}$ is the mean PNC of replicates 1 and 2 for *Lab*) for PNC within instrument groups. The number in the table is the mean CV (mCV) for n laboratories that reported PNCs in that bin using the technique. *NA* indicates that value is not available. The distributions of CVs for each instrument group and bin are shown in Fig. 4.

Instrument	Bin1		Bin2		Bin3		Bin4		Bin5	
	n	mCV	n	mCV	n	mCV	n	mCV	n	mCV
PTA	18	36 %	18	13 %	18	13 %	18	29 %	12	74 %
RMM	*NA*	*NA*	1	13 %	5	6 %	7	17 %	7	20 %
ESZ	2	29 %	2	29 %	4	17 %	4	12 %	4	22 %
HPC	*NA*	*NA*	*NA*	*NA*	1	3 %	3	20 %	3	9 %

Table 4
Interlaboratory variability: Mean PNC (mL^{-1}) and coefficients of variation for instrument groups. The CV was calculated based upon the laboratory mean values calculated for the Samples 1 and 2. The *n* is the same as reported in Table 3 for each group, bin combination. *NA* indicates that value is not available.

Instrument	Bin1		Bin2		Bin3		Bin4		Bin5	
	PNC	CV	PNC	CV	PNC	CV	PNC	CV	PNC	CV
PTA	8.1×10^8	189 %	1.2×10^9	124 %	6.6×10^8	114 %	9.7×10^7	133 %	2.9×10^6	113 %
RMM	*NA*		1.7×10^6	*NA*	3.1×10^8	58 %	3.3×10^7	87 %	1.5×10^6	38 %
ESZ	3.9×10^8	104 %	3.0×10^8	45 %	1.2×10^8	80 %	2.5×10^7	76 %	1.4×10^6	13 %
HPC	*NA*		*NA*		9.8×10^5	*NA*	1.4×10^6	164 %	1.3×10^6	25 %

the intralaboratory CVs over 1.4 times smaller than the interlaboratory CVs. This is shown graphically in Supplemental Figure S5 by using Youden plots, which provide a convenient display of intralaboratory and interlaboratory variability. The differences in the two variances can be attributed to the intralaboratory measurements being performed within a short time interval on the same instruments with, generally, the same analyst handling samples and setting instrument parameters for data acquisition and analysis. The use of software-selected data acquisition and analysis parameters, a feature with some instruments, could be a potential source for relatively high intralaboratory CVs. That is, if the instrument software selects different parameters between the paired samples (for example, the heterogeneous nature of the sample may yield sufficient differences if an instantaneous population distribution is evaluated to select acquisition parameters), then differences in the resultant CDDs could be expected, which would result in relatively high CVs for that laboratory. As shown in Fig. 4, most of the mean intralaboratory CVs are less than 30 %; however, for the PTA group, three of the bins have mean CVs of 30 % or more. These numbers indicate some inconsistencies within laboratories when measuring the sample at the highest and lowest size and particle number concentration ranges. This could be related to the PNC for particles in those size regimes: that is, the smallest particles ($d < 0.14\ \mu m$) with a relatively high PNC and the largest particles ($d \geq 0.86\ \mu m$) with a relatively low PNC may be outside of the optimal counting window for an instrument and a single set of measurement/analysis parameters.

Discussion

The ILC discussed here was intended to explore the responses from varied instruments to a sample that contained a mixture of particles with diameters that varied across the sub-micrometer range. Because of the range of particle sizes and the large variety of instruments included in the study, we anticipated that, as seen in the results, some of the methods would be incapable of resolving the smallest particle sizes in the study. Depending on the instrumental approach, the lower size limits can be attributed to, for example, insufficient particle mass to change cantilever frequency (RMM), insufficient particle volume to change electrical resistance (ESZ), or insufficient optical size or light scattering for video microscopy or holographic tracking. The study sample included particles as large as 1 μm in the samples, which tested the ability of the instruments to obtain accurate particle counts of smaller particles in the presence of larger particles. Our sample also used a relatively large number of spheres with $d < 0.5\ \mu m$ to give a more demanding test of the ability to discriminate details of the size distribution (e.g., number of count peaks and their positions). Samples containing individual sub-populations were not included in this study to avoid biasing the analysis of the unknown multi-modal sample.

While our sample was composed of discrete particle populations that can yield distinct peaks in the particle size distribution, the size distribution was intended to approximate a natural distribution of particle sizes (i.e., decreasing PNC with increasing particle size). Because the sub-population particle counts decreased with increasing particle size, we note that the number of the largest particles in the sample could fall below the lower limit of quantification for certain instruments, especially if diluted. The sphere populations were based upon PMMA, which has a density, $\rho \approx 1.19$ g/mL and a refractive index, $n \approx 1.49$ at 633 nm, though some variability can be expected because of differences in, for example, cross linking.[35] One sphere population of silica with a nominal diameter of 0.195 μm was used in the mixture as well, which provided a sub-population with a different density ($\rho \approx 2$ g/mL) and refractive index ($n \approx 1.41$ at 633 nm).[36] For comparison, the density and refractive index of water are, respectively, $\rho = 0.998$ g/mL and $n = 1.33$ at 20 °C and 633 nm.[37] While not explicitly explored in this study, use of a combined mixture of silica and PMMA allows for assessment of the ability of counting methods to work with samples that are heterogeneous in density and refractive index. While protein drug products are not typically monitored for sub-micrometer particles, when observed, the particles can be heterogeneous in composition. For example, they may be a mixture of proteinaceous species, silicone oil droplets, rubber, plastic, metal pieces, etc. that differ in density and refractive index.[8,11] Given that the sample was predominantly composed of PMMA spheres, it was recommended that participants use the PMMA density for converting RMM data to size. As noted above in the experimental section, the silica may influence particle counts with a peak at $\approx 0.35\ \mu m$, with the peak shift observed in the averaged RMM data, but not in all individual plots (Figs. 1 and 2).

The interlaboratory differences observed in the particle counts and peak positions can be attributed, at least in part, to different instruments (different models, manufacturers) used even within a given instrument group, as well as instrumental configurations (e.g., orifices for ESZ instruments, cantilevers for RMM instruments, lasers and other optics, including cameras (e.g., using CCD (charge-coupled device) or CMOS (complementary metal oxide semiconductor) sensors), for the PTA and OTH groups), and data acquisition and analysis settings in the instrumental software. These large differences in particle counts observed at the upper and lower size limits of the different datasets suggest that instruments may have been optimized for a subset of the sample size range, thus missing particle counts beyond that optimal range. The missed particle counts in a distribution could potentially include particles of both smaller and larger sizes. The mean distributions shown in Fig. 2 suggest that the instruments are in principle able to cover a broad size range, but broad coverage may require multiple runs with more extensive instrument optimization for different size subranges and different types of samples. Thus, different measuring protocols would be necessary. Using a system check sample representative of the test sample for configuring the instrument setup could address this issue, or at least alert users to the potential for missed particles. Consequently, measuring time will increase, including larger sample volumes, because each sample would need to be analyzed for a specific size range, although the same instrument/method would be used. Analyses on series of dilutions or with systematically adjusted settings to optimize an instrument for the extreme ends of the sample may be necessary to capture a more complete picture of the full distribution. Note also that the manner in which the distributions are presented graphically

can emphasize or hide aspects of the distributions (e.g., low counts for large particles hidden on a linear scale in Supplemental Figure S2; emphasizing larger particles with a volume-based count as seen in Supplemental Figure S6). Users in certain application areas, such as environment or food, may be more interested in, for example, the volume of materials in samples, where contributions from larger particles will have greater impact on the amount of material in a sample (by mass or by volume).

In this ILC there were many potential sources of variability. Beyond limited harmonization from the guidance and instructions provided to all participants for sample handling and measurements, each participant was free to develop and apply their own approaches to the sample, which included the instrument, its configuration and setup, and sample analysis. Because some of these methods may not be used in a routine fashion, method qualification may be limited. Each of these categories has the potential to introduce variability and uncertainties in the results, both within and between the instrument groups. Instrument configurations can be quite different even within the specific groups: PTA instruments used one, two, or three lasers with varying wavelengths; RMM instruments used cantilevers with different lower mass limits; and ESZ instruments used orifices with differently sized openings. Instrument settings could also vary widely owing to differences in specific laboratory procedures for measuring samples with particles in this size regime (e.g., optimizing for smaller or larger particles). The sample handling techniques, including any dilutions, also varied between laboratories, which can introduce variability to the reported results. By restricting harmonization to assuring sample homogeneity (by the Youden method) and providing sample-handling guidance, but not harmonizing the implementation of the methods, insight was gained into measurement consistency in actual practice, both within and between laboratories. With the use of standardized and more prescriptive sample handling procedures, perhaps broken down by instrument type, a reduction of the variability within the instrument groups could be expected. Such trends are often seen in ILCs with multiple rounds of sampling.[21,25,26]

In general, the sample analyses in terms of peak positions and PNCs have been discussed only within instrument groups. Because the methods are orthogonal and, as noted above, measuring different aspects of particle size (e.g., hydrodynamic diameters, mass- or volume-based diameters, equivalent spherical diameters), and given the variability within groups, it is challenging to make any direct comparisons. Furthermore, the effective size ranges between (and within) the instrument groups vary, so differences in PNC are also difficult to reconcile. However, we do note that for Bin5, there appears to be some agreement on peak position (Fig. 2) and PNC (Table 4) between the RMM, ESZ, HPC techniques, with relatively low interlaboratory CVs.

The results from this study can be compared with other ILCs considering similar samples or measurement approaches,[10,21-27] and also smaller studies looking at, for example, the differences in performance between instrument types.[14,28-31,38] Many of these did not evaluate the particle number concentrations, but focused on other aspects (primarily particle size, but also zeta potential).[22-26,28] For particle sizing, the ILCs generally had good agreement, especially if there was a second round of testing with established standard operating procedures for sample handling, data acquisition and analysis based upon the results of the first round of tests. For example, a study examining the use of PTA to measure the size of polystyrene beads (mono- and bi-modal samples) showed average CVs of 38 % in round one, which dropped to 4 % by round 4.[22] Similar trends were noted in other studies using dynamic light scattering or differential centrifugal sedimentation to measure the size of silica or polystyrene (PS) beads and nanoparticles.[25,26] A study that looked at comparing PTA and ESZ with atomic force microscopy (AFM), electron microscopy (EM), and synchrotron small angle X-ray scattering (SAXS) size measurements of PS and silica beads found that the PTA and ESZ sizes were within 3 % on the PS and within 15 % for silica beads.[23] Another trend noted was that polydispersity (of either single or multi-modal populations) caused challenges in sizing resolution and reproducibility.[25,28,30]

With respect to particle number concentration, an ILC looking at counts for a larger polydisperse sample (sub-visible, 1 μm < d < 25 μm ethylene tetrafluoroethylene (ETFE) particles) found CVs for mean cumulative PNCs ranging from 9 % to 86 % depending on the particle size range and instrument type (light obscuration, ESZ, or flow imaging).[21] On the smaller end of the particle sizing range, counts of gold nanoparticles (d = 30 nm, 60 nm) were the focus of an interlaboratory study that used, among other techniques, PTA.[27] In that study, the established methods of EM and single-particle inductively couple plasma-mass spectrometry agreed on PNC within 20 %, while other techniques could vary by a factor of three.[27] For studies that more directly targeted counting in the sub-micrometer size range, one focused on the use of PTA to size and quantify extracellular vesicles.[14] For a single instrument, CVs averaged 3 % to 4 % for size and 10 % to 14 % for PNC, while across multiple instruments size mismatch ranged up to 22 % and PNC mismatch up to 102 %.[14] Two other studies compared various sub-micrometer instruments (PTA and RMM in both studies, ESZ in one) in measurements of beads, proteins (drug products), and related materials,[10,31] and another study compared PTA, RMM, and quantitative laser diffraction instruments in measurements of aggregated proteins.[38] The (intralaboratory) comparison reported on by Grabarek et al. included measurements of PS distributions at sizes of 297 nm, 495 nm, and 799 nm, covering a narrower size range than the present work.[31] Similar to the findings here, their study found that PTA lost sensitivity toward smaller and larger particles, and shifts in particle sizes compared to ESZ and RMM techniques.[31] The ILC reported by Hubert et al. looked at, among other samples, PS beads and a protein control sample and found that sizing for the beads was generally within 10 %.[10] PNCs and standard deviations for up to six laboratories measuring the protein control sample were calculated to be $(5.4 \pm 3.2) \times 10^8$ mL^{-1} and $(6.9 \pm 2.5) \times 10^6$ mL^{-1} for PTA and RMM, respectively, with relative standard deviations lower than seen in our current study.[10] Similar to our findings, the overall PNCs for RMM were lower than those measured by PTA, even considering only particles with diameter greater than 0.4 μm.[10] The general messages from these studies parallel the results presented from our study here: while sizing of monodisperse particles (not included in this study) has been relatively robust, multi-modal and polydisperse samples were challenging both to size and to count, especially at the extremes of the sample or instrumental ranges.

Conclusions and Perspectives

The strength of the study is built upon the combination of a defined polydisperse test sample, a varied selection of instrument types and approaches, and a large participant group across the biopharmaceutical industry, instrument manufacturers, government agencies, and academia. The sample contained a mixture of particles with peak diameters that ranged from ≈ (0.1 to 1) μm and was intended to explore the responses from varied instruments. While composed of discrete particle populations that yield distinct peaks in the particle size distribution, the size distribution was intended to approximate a natural distribution of particle sizes (i.e., decreasing PNC with increasing particle size). It is also relevant that the sample materials, PMMA and silica, have refractive indices close to those of protein aggregates and other biological particles since many of the measurement approaches in the sub-micrometer size regime rely on light scattering.

The dataset generated through this study provides a snapshot of approaches for characterizing the particle size distribution of

dispersions in the under-studied sub-micrometer regime with sizes between 0.1 μm and $\approx$ 1 μm. For measurement of PNC, the mean intralaboratory CV (Table 3) comprised, on average, 37 % of the interlaboratory CV (Table 4) for a particular instrument group and size bin. Individual laboratory sets show the capability for resolving peaks in the size distribution, but there is poor agreement on PNC peak location below 0.5 μm; conversely, for larger particle sizes, there is better agreement on the peak position. Distributions from the RMM, ESZ and OTH instrument groups show a distinct peak for the 1 μm particle population. While individual laboratory distributions tend to show drop-offs at either end of the size range, the mean instrument distributions shown in Fig. 2 demonstrate that broader coverage is possible. We note that since the time when the measurements were made, updates may have been made to both instruments and software packages used for data acquisition and analysis.

These observations suggest opportunities for moving measurements of particles in this size regime toward better agreement. In particular, the capability to assess the sensitivity of an instrument with a given configuration (e.g., measurement cell, operator-controlled data acquisition and analysis parameters) across the size range of interest would be beneficial. Such information would yield a better understanding of instrumental limits and could lead to the development of operational protocols that would ensure that the full size range of interest is adequately covered. For example, a procedure can be envisioned that combines multiple runs with systematically adjusted settings optimized for different particle-size subranges. This type of instrument check and protocol development or method qualification could be enabled by multi-modal samples similar to the sample used in this study. Furthermore, if multi-modal (certified) reference materials are quantified for size (and polydispersity) and particle number concentration, then standardization of PNC would be possible as well. As agreement between measurements in this size regime improves, next-generation reference materials might contain non-spherical particles to better mimic real-world samples. To facilitate such an approach, however, there is a need to develop and demonstrate orthogonal measurements with limited bias that are traceable to the International System of Units that can be applied to both size and quantification of particles in this sub-micrometer size regime.

Supplementary Materials

The supplemental material contains several tables and figures, with associated text, as referenced in the text above. In addition, the full dataset is available at https://doi.org/10.18434/mds2-2486. The dataset is organized by instrument group, and each instrument group data file contains each distribution in the “rounded log” bins and in the five wider bins as concentration distribution densities. The cumulative particle number concentration (PNC) for each distribution is also given. The mean distributions with standard deviations and standard error are given for each instrument group (PTA, RMM, ESZ, HPC).

Supplementary material associated with this article can be found in the online version at doi:10.1016/j.xphs.2021.11.006.

Declaration of Competing Interest

The authors declare the following financial interests/personal relationships which may be considered as potential competing interests:

N. Do is an employee of Spectradyne LLC, which manufactures and sells microfluidic resistive pulse sensing-based instrumentation for particle quantification.

D. Grier is a founder of Spheryx, Inc., the company that manufactures the xSight instrument that was used for part of the NYU study.

J. Hadley was employed at Malvern Panalytical, which develops and sells the Archimedes and LM10, LM14, LM20, NS300, and NS500 instruments used in this study.

C. Probst was employed by Luminex Corporation, the manufacturer of the Amnis® CellStream® and FlowSight® that were used in this study.

During this study J. Tatarkiewicz was employed by MANTA Instruments, Inc. which since then was acquired by HORIBA Scientific, Inc. The measurements were done using ViewSizer 3000 instrument.

Alpha Nano Tech LLC is a Contract Research Organization; it has actual contracts with Particle Metrix Inc., as well as with other instruments vendors, and provides services for the companies on request. In general, Alpha Nano Tech LLC has contracts with Particle Metrix and special terms on acquiring instruments. Alpha Nano Tech provides services on variety of instruments/techniques, including those which compete with each other.

Spheryx Inc. sells the Holographic Characterization Instrument (xSight and xCell8) used in this publication. We also hold the patents associated to this technology.

Yokogawa Fluid Imaging Technologies, Inc. develops and sells the FlowCam® Nano flow imaging microscope used in this study.

All other authors declare that they have no known competing financial interests or personal relationships that could have appeared to influence the work reported in this paper.

Acknowledgements

We thank Blaza Toman from the Statistical Engineering Division at NIST for initial discussions on the datasets, Jonathan Mehtala from Malvern Panalytical for assisting with PTA measurements, Franklin Monzon (data analysis and manuscript review), Jean-Luc Fraikin (data analysis and manuscript review), and Lew Brown (manuscript review) from Spectradyne, LLC for their assistance.

Funding

This study was sponsored at Alpha Nano Tech LLC by Particle Metrix Inc.

Research reported in this publication at Spheryx Inc was supported by the National Science Foundation under Award Number 1631815, and the National Center For Advancing Translational Sciences of the National Institutes of Health under Award Number R44TR001590.

Work by D. Grier at NYU was supported by the National Science Foundation under Award Number DMR-2027013. The xSight particle characterization instrument and LS Spectrometer used for this work were acquired as shared facilities by the Materials Research Science and Engineering Center program of the NSF under Award Number DMR-1420073. The work of A. D. Hollingsworth was partially supported by NASA award number NNX13AR67G.

For the remaining institutions, this research did not receive any specific grant from funding agencies in the public, commercial, or not-for-profit sectors.

References

1. Carpenter JF, Randolph TW, Jiskoot W, et al. Overlooking subvisible particles in therapeutic protein products: gaps that may compromise product quality. *J Pharm Sci*. 2009;98(4):1201–1205.
2. Narhi LO, Schmit J, Bechtold-Peters K, Sharma D. Classification of protein aggregates. *J Pharm Sci*. 2012;101(2):493–498.
3. Wang W, Singh SK, Li N, Toler MR, King KR, Nema S. Immunogenicity of protein aggregates—concerns and realities. *Int J Pharm*. 2012;431(1):1–11.
4. Roberts CJ. Protein aggregation and its impact on product quality. *Curr Opin Biotechnol*. 2014;30:211–217.
5. Pham NB, Meng WS. Protein aggregation and immunogenicity of biotherapeutics. *Int J Pharm*. 2020;585: 119523.

6. Amin S, Barnett GV, Pathak JA, Roberts CJ, Sarangapani PS. Protein aggregation, particle formation, characterization & rheology. *Curr Opin Colloid Interface Sci*. 2014;19(5):438–449.
7. Das TK. Protein particulate detection issues in biotherapeutics development—current status. *AAPS PharmSciTech*. 2012;13(2):732–746.
8. Ripple DC, Dimitrova MN. Protein particles: What we know and what we do not know. *J Pharm Sci*. 2012;101(10):3568–3579.
9. Kijanka G, Bee JS, Korman SA, et al. Submicron size particles of a murine monoclonal antibody are more immunogenic than soluble oligomers or micron size particles upon subcutaneous administration in mice. *J Pharm Sci*. 2018;107(11):2847–2859.
10. Hubert M, Yang DT, Kwok SC, et al. A multicompany assessment of submicron particle levels by nta and rmm in a wide range of late-phase clinical and commercial biotechnology-derived protein products. *J Pharm Sci*. 2020;109(1):830–844.
11. Messick S, Saggu M, Ríos Quiroz A. Chapter 11: Particles in biopharmaceuticals: causes, characterization, and strategy. In: Jameel F, Skoug JW, Nesbitt RR, eds. *Development of Biopharmaceutical Drug-Device Products*. Cham: Springer International Publishing; 2020:251–264.
12. Jarzębski M, Bellich B, Białopiotrowicz T, Śliwa T, Kościński J, Cesàro A. Particle tracking analysis in food and hydrocolloids investigations. *Food Hydrocolloids*. 2017;68:90–101.
13. Slütter B, Jiskoot W. Sizing the optimal dimensions of a vaccine delivery system: a particulate matter. *Expert Opin Drug Deliv*. 2016;13(2):167–170.
14. Vestad B, Llorente A, Neurauter A, et al. Size and concentration analyses of extracellular vesicles by nanoparticle tracking analysis: a variation study. *J Extracell Vesicles*. 2017;6:(1) 1344087.
15. van der Pol E, Coumans FAW, Grootemaat AE, et al. Particle size distribution of exosomes and microvesicles determined by transmission electron microscopy, flow cytometry, nanoparticle tracking analysis, and resistive pulse sensing. *J Thromb Haemost*. 2014;12(7):1182–1192.
16. Ríos Quiroz A, Finkler C, Huwyler J, Mahler H-C, Schmidt R, Koulov AV. Factors governing the accuracy of subvisible particle counting methods. *J Pharm Sci*. 2016;105(7):2042–2052.
17. Sung JJ, Pardeshi NN, Mulder AM, et al. Transmission electron microscopy as an orthogonal method to characterize protein aggregates. *J Pharm Sci*. 2015;104(2):750–759.
18. Hodoroaba V-D, Unger WES, Shard AG. *Charaterization of Nanoparticles: Measurement Processes for Nanoparticles*. 1st ed. Amsterdam: Elsevier Inc; 2019.
19. Merkus HG. *Particle Size Measurements*. 1st ed. Dordrecht: Springer; 2009.
20. Gross-Rother J, Blech M, Preis E, Bakowsky U, Garidel P. Particle detection and characterization for biopharmaceutical applications: current principles of established and alternative techniques. *Pharmaceutics*. 2020;12(11):1112.
21. Ripple DC, Montgomery CB, Hu Z. An interlaboratory comparison of sizing and counting of subvisible particles mimicking protein aggregates. *J Pharm Sci*. 2015;104(2):666–677.
22. Hole P, Sillence K, Hannell C, et al. Interlaboratory comparison of size measurements on nanoparticles using nanoparticle tracking analysis (NTA). *J Nanopart Res*. 2013;15(12):2101.
23. Nicolet A, Meli F, van der Pol E, et al. Inter-laboratory comparison on the size and stability of monodisperse and bimodal synthetic reference particles for standardization of extracellular vesicle measurements. *Meas Sci Technol*. 2016;27(3):035701.
24. Lamberty A, Franks K, Braun A, Kestens V, Roebben G, Linsinger TPJ. Interlaboratory comparison for the measurement of particle size and zeta potential of silica nanoparticles in an aqueous suspension. *J Nanopart Res*. 2011;13(12):7317–7329.
25. Roebben G, Ramirez-Garcia S, Hackley VA, et al. Interlaboratory comparison of size and surface charge measurements on nanoparticles prior to biological impact assessment. *J Nanopart Res*. 2011;13(7):2675.
26. Langevin D, Lozano O, Salvati A, et al. Inter-laboratory comparison of nanoparticle size measurements using dynamic light scattering and differential centrifugal sedimentation. *NanoImpact*. 2018;10:97–107.
27. Petersen EJ, Montoro Bustos AR, Toman B, et al. Determining what really counts: modeling and measuring nanoparticle number concentrations. *Environmental Science: Nano*. 2019;6(9):2876–2896.
28. Anderson W, Kozak D, Coleman VA, Jämting ÅK, Trau M. A comparative study of submicron particle sizing platforms: Accuracy, precision and resolution analysis of polydisperse particle size distributions. *J Colloid Interface Sci*. 2013;405:322–330.
29. Panchal J, Kotarek J, Marszal E, Topp EM. Analyzing subvisible particles in protein drug products: a comparison of dynamic light scattering (DLS) and resonant mass measurement (RMM). *The AAPS Journal*. 2014;16(3):440–451.
30. Gross J, Sayle S, Karow AR, Bakowsky U, Garidel P. Nanoparticle tracking analysis of particle size and concentration detection in suspensions of polymer and protein samples: influence of experimental and data evaluation parameters. *Eur J Pharm Biopharm*. 2016;104:30–41.
31. Grabarek AD, Weinbuch D, Jiskoot W, Hawe A. Critical evaluation of microfluidic resistive pulse sensing for quantification and sizing of nanometer- and micrometer-sized particles in biopharmaceutical products. *J Pharm Sci*. 2019;108(1):563–573.
32. International Organization for Standardization. *Preparation of Particulate Reference Materials — Part 1: Polydisperse Material Based on Picket Fence of Monodisperse Spherical Particles*. Geneva, Switzerland: ISO; 2017.
33. Certain commercial equipment, instruments, or materials are identified in this paper in order to specify the experimental procedure adequately. Such identification is not intended to imply recommendation or endorsement by NIST, nor is it intended to imply that the materials or equipment identified are necessarily the best available for the purpose.
34. Hole P. Chapter 3.1.2 - Particle tracking analysis (PTA). In: Hodoroaba V-D, Unger WES, Shard AG, eds. *Characterization of Nanoparticles*. Cambridge, MA: Elsevier; 2020:79–96.
35. Zhang X, Qiu J, Li X, Zhao J, Liu L. Complex refractive indices measurements of polymers in visible and near-infrared bands. *Appl Opt*. 2020;59(8):2337–2344.
36. Kimoto S, Dick WD, Hunt B, Szymanski WW, McMurry PH, Roberts DL, Pui DYH. Characterization of nanosized silica size standards. *Aerosol Sci Technol*. 2017;51(8):936–945.
37. Rumble JR, ed. *CRC Handbook of Chemistry and Physics. 101st (Internet Version 2020)*. Boca Raton, FL: CRC Press/Taylor & Francis; 2020.
38. Yoneda S, Niederleitner B, Wiggenhorn M, et al. Quantitative laser diffraction for quantification of protein aggregates: comparison with resonant mass measurement, nanoparticle tracking analysis, flow imaging, and light obscuration. *J Pharm Sci*. 2019;108(1):755–762.